



# The Impact of Climate Change on Extreme Winds over Northern Europe According to CMIP6

Xiaoli Guo Larsén<sup>1</sup>, Marc Imberger<sup>1</sup>, Ásta Hannesdóttir<sup>1</sup>, and Andrea N. Hahmann<sup>1</sup>

<sup>1</sup>Department of Wind and Energy Systems, Technical University of Denmark

**Correspondence:** Xiaoli Guo Larsén (xgal@dtu.dk)

**Abstract.** We study the possible effect of climate change on the extreme wind over Northern Europe using data from 18 models of the Sixth Phase of the Coupled Model Intercomparison Project (CMIP6) and the high-emission SSP585 scenario. We use the spectral correction method to correct the 6-hourly wind speeds and calculate the 50-year wind at an equivalent temporal resolution of 10 minutes, consistent with the International Electrotechnical Commission (IEC) standard. We assess the quality of the CMIP6 wind data during the historical period through comparison to the spatial patterns of the extreme wind in three reanalysis data. We obtain the possible effect of climate change through the comparison of the extreme wind parameters, including the 50-year wind and the 95%-percentile of the wind speed, and the change in turbine class at 50 m, 100 m and 200 m, between a near future period (2020–2049) and the historic period (1980–2009). The analysis shows an overall increase in the extreme winds in the North Sea and the southern Baltic Sea, but a decrease over the Scandinavian Peninsula and most of the Baltic Sea. However, the analysis is inconclusive to whether higher or lower classes of turbines will be installed in this area in the future.

## 1 Introduction

Extreme winds can cause great loss to society and the 50-year wind,  $U_{50}$ , a common measure of extreme winds, is one of the most important siting parameters that needs to be estimated when planning regional wind energy development. An accurate estimation of the extreme wind can help to harvest more electricity from winds, while avoiding placing the turbines in dangerous places, and to avoid or over-design of the wind turbines; it is directly related to the Levelized Cost Of Energy (LCOE) and the cost of climate mitigation.

We live in a world where climate is changing and where the damage to society from extreme winds is rising every year (MunichRe, 2011). The scale and speed of wind energy development and deployment have never been so large and it will continue in the future (GWEC, 2022). It is thus a relevant question to ask how climate change (CC) will impact extreme winds in the future and what this change implies for the cost of wind energy development.



While observed trends and the effect of CC has been studied extensively for extreme temperature and precipitation (e.g. IPCC, 2021, Chapter 11), studies on extreme winds are fewer. For the studies of extreme wind, data from various models with a variety of temporal and spatial resolution have been used. Reanalysis data has been a popular choice for extreme wind estimation due to its global coverage and long-term availability, including ECMWF reanalysis ERA-40 (e.g. Della-Marta et al., 2009), reanalysis from National Centers for Environmental Prediction and the National Center for Atmospheric Research (NCEP/NCAR) (e.g. Larsén and Mann, 2009), NOAA 20th century reanalysis (e.g. Donat et al., 2011), the 5th generation reanalysis from ECMWF ERA5 (e.g. Pryor and Bartelmie, 2021; Imberger and Larsén, 2022), Climate Four-Dimensional Data Assimilation CFDDA (e.g. Hansen et al., 2016), Climate Forecast System Reanalysis I CFSR (e.g. Larsén and Kruger, 2014) and Modern-Era Retrospective analysis for Research and Applications MERRA2 (e.g. Imberger and Larsén, 2022). The temporal resolution of these data ranges from 1 to 6 hours, and the spatial grid spacing from about 25 km to a couple of hundreds of kilometers. This resolution is too coarse and not ideal for site-specific extreme wind calculations. Using data from mesoscale model simulations is expected to improve the extreme wind estimation, as shown in e.g. Bastine et al. (2018) and Larsén et al. (2021), where data from the Weather Research and Forecasting (WRF) model with spatial grid spacing of 3 km were used. The only global coverage of extreme wind that has applied microscale modeling with spatial grid spacing of 275 m has been created within the in the Global Atlas for Siting Parameters (GASP) project (Larsén et al., 2022).

For extreme winds, many of the studies focus on the estimation of extreme winds using historical data, rather than about the impact of CC. In recent decades, Regional Climate Models (RCMs) have been used to study the impact of CC on extreme wind. These include, for example, the PRUDENCE project (Prediction of Regional Scenarios and Uncertainties for Defining European Climate Change Risks and Effects), a EU Framework Program 6 project that ended in 2004 (PRU), ENSEMBLES (Ensemble-Based Predictions of Climate Changes and their Impacts), a successor to PRUDENCE which finished in 2009 (ENS) and CORDEX (Coordinated Regional Downscaling Experiment, Giorgi and Gutowski, 2015), based on infrastructure known from the Fifth Phase of the Coupled Model Intercomparison Project (CMIP5; Taylor et al., 2012). The RCMs included in the PRUDENCE project have a spatial grid spacing of 50 km, ENSEMBLES 25 km and CORDEX 12 km. With PRUDENCE, Beniston et al. (2007) (with both high and low emission scenarios A2 and B2), Schwierz et al. (2010) (with SRES A2 scenario), and Rockel and Woth (2007) (also with SRES A2 scenario) studied the CC on extreme wind using 90th, 98th and 99th percentiles of wind speed, as well as gust and the  $T$ -year return wind speed for the period 1961–1990 vs. 2071–2100. They found that these models suggest an increase in extreme wind in Central Europe in the future due to climate change. With ENSEMBLE, Donat et al. (2011) (with SRES A1B scenario) analyzed the 98th percentile of wind speed and found an increase in Northern Europe and a decrease in the Mediterranean Sea; Pryor et al. (2012) (with SRES A1B scenario) analyzed  $U_{50}$  and found similar change in Northern Europe in line with findings by Donat et al.; Clausen et al. (2012) (with SRES A1B scenario) analyzed four ensemble model members and calculated the 90th, 95th and 99th percentiles,  $U_{50}$  and the linear trend at hub height of 100 m, and found that in Europe, there is no significant change in  $U_{50}$  in majority of the grid cells by the middle of the century, while towards the end of the century, there is an increasing number of grid cells that show increases in  $U_{50}$  larger than the natural variability. With CORDEX, Outten and Sobolowski (2021) (with RCP8.5 scenario) calculated 10, 20, 30, 50



and 100-year return wind values for Europe for three periods 2011–2040, 2041–2070 and 2071–2100 and they found an overall increase in extreme wind in the future, for both Northern and Southern Europe.

In comparison with estimations from ENSEMBLE data, Outten and Sobolowski (2021) found that the 12 km resolution CORDEX data provides more details over complicated landscape e.g. land and coastal areas, with enhanced extreme events. The typical resolution of RCMs, which is on the order of tens of kilometers on hourly basis, is not high enough for the purpose of site specific estimation of extreme wind, due to the ever-present smoothing effect in numerical models (Larsén et al., 2012). These data are however still useful to identify trends and changes in the extreme wind estimation.

The CMIP6 project is the sixth phase and most recent phase of the CMIPs (Eyring et al., 2016). It used World Climate Research Programme (WCRP) Grand science Challenges (GCs) as the scientific backdrop of its experiment design. These GCs constitute a main component of the WCRP strategy to accelerate progress in climate science (Brasseur and Carlson, 2015), with one of the seven subjects particularly on climate extremes: “assessing climate extremes, what controls them, how they have changed in the past and how they might change in the future”. A parallel study, Hahmann et al. (2022), used this data set to examine the CC effect on wind resources for Northern Europe.

Previous studies on the impact of CC on the extreme wind using the several generations of RCMs have not reached a consensus. In this study, we make use of the CMIP6 data to study the CC impact on the extreme wind. To relate our calculation and analysis to the IEC standard for turbine design (IEC, 2019), we downscale the CMIP6 time series of wind speed in the temporal domain using a fast and simple spectral model. This method, called the spectral correction (SC) method, produces an equivalent 10-min temporal resolution and is introduced in section 2.3. Data are introduced in section 2, followed by the results in section 3. The discussion of the results and the conclusions are in section 4 and section 5, respectively.

## 2 Data and methods

We use the output from CMIP6 models to assess the CC impact on the extreme wind over two periods: the historical period (his-Period, 1980–2009) and the near future period (fut-Period, 2020–2049) from the CMIP6 historical and SSP585 simulations, respectively (Eyring et al., 2016). These two periods are relevant for a turbine’s life time of 20–30 years for a wind farm being planned in 2020. When using climate model output, it is always a challenge to quantify or qualify the systematic signals and uncertainties. To help qualifying the model reliability, we compare the estimate of  $U_{50}$  from CMIP6 his-Period to that from the reanalysis data. The comparison results will be taken into consideration when we perform the analysis of CC.

The CMIP6 data are introduced in section 2.1 and the reanalysis data in section 2.2. Both data will be processed using the SC method when calculating  $U_{50}$ , which is described in section 2.3.

### 2.1 The CMIP6 data

To be consistent with the study of wind resource using CMIP6 data in Hahmann et al. (2022), we use the 18 models listed in Table 1. Among the many CMIP6 models these 18 are chosen because of the availability of model outputs of surface pressure, temperature and humidity in addition to the wind components  $u$  and  $v$  at the raw model level for the simulations of the historical



**Table 1.** Models in the CMIP6 archive used in this study.

No.	Model	Approx. grid spacing	Number of vertical levels	Reference
1	ACCESS-CM2	$1.25^\circ \times 1.875^\circ$	85	Tilo et al. (2020)
2	CanESM5	$2.8125^\circ \times 2.79^\circ$	49	Swart et al. (2019)
3	CESM2	$1.25^\circ \times 0.94^\circ$	32	Danabasoglu et al. (2020)
4	CMCC-CM2-SR5	$1.25^\circ \times 0.94^\circ$	30	Cherchi et al. (2019)
5	CNRM-CM6-1	$1.4^\circ \times 1.4^\circ$	91	Voltaire et al. (2019)
6	CNRM-ESM2-1	$1.4^\circ \times 1.4^\circ$	91	Séférian et al. (2019)
7	HadGEM3-GC31-LL	$1.875^\circ \times 1.25^\circ$	85	Sellar et al. (2020)
8	HadGEM3-GC31-MM	$0.833^\circ \times 0.556^\circ$	85	Sellar et al. (2020)
9	IPSL-CM6A-LR	$2.5^\circ \times 1.27^\circ$	91	Boucher et al. (2020)
10	MIROC6	$1.4^\circ \times 1.4^\circ$	81	Tatebe et al. (2019)
11	MIROC-ES2L	$2.8125^\circ \times 2.79^\circ$	40	Hajima et al. (2020)
12	MPI-ESM1-2-HR	$1.875^\circ \times 1.865^\circ$	47	Müller et al. (2018)
13	MPI-ESM1-2-LR	$0.9375^\circ \times 0.935^\circ$	85	Mauritsen et al. (2019)
14	MRI-ESM2-0	$1.125^\circ \times 1.121^\circ$	80	Kawai et al. (2019)
15	NESM3	$1.875^\circ \times 1.865^\circ$	47	Yang et al. (2020)
16	NorESM2-LM	$2.5^\circ \times 1.895^\circ$	32	Seland et al. (2020)
17	NorESM2-MM	$1.25^\circ \times 0.942^\circ$	32	Seland et al. (2020)
18	UKESM1-0-LL	$1.875^\circ \times 1.25^\circ$	85	Sellar et al. (2020)

(1980–2014) and SSP585 (2015–2050) scenarios. These additional data are needed to convert the wind from model levels to heights about model ground levels, e.g. the turbine hub height. Wind speeds above ground level at 50 m, 100 m and 200 m are obtained through vertical logarithmic height interpolation; these heights are relevant for modern turbine sizes.

To reduce the data download volume, the CMIP6 model data was cropped to approximately cover the area  $-10 - 30^\circ\text{E}$  and  $50 - 70^\circ\text{N}$ , same as in Hahmann et al. (2022). The 18 models are labeled with numbers in Table 1, together with the corresponding model atmospheric grid spacing and the number of vertical model levels. All data are available on 6-hour basis. Details of these models can be found in the references.

## 2.2 The reanalysis data

The reanalysis data is used to assess the reliability of the CMIP6 wind speeds in describing extreme winds in this region by qualitatively examining the spatial distribution and patterns of  $U_{50}$ .

Three reanalysis data sets are used: (1), the CFSR data (Saha et al., 2010) available at hourly temporal resolution with a grid spacing of about 40 km; (2), the MERRA2 data (Gelaro et al., 2017) available hourly with a grid spacing of  $0.5 \times 0.625^\circ$ ; (3),



the ERA5 (Hersbach et al., 2020) available hourly with a grid spacing of about 27 km. We calculate  $U_{50}$  using the his-Period with the three data sets with the SC method.

In the three reanalysis data sets, wind speed diagnostics are available at different heights: 10 m (CFSR), 10 m and 50 m (MERRA2), and at 10 m and 100 m (ERA5). Optimally a single common height for comparison to hub height is necessary. 105 But, the extrapolation of the wind speeds from a height, i.e., 10 m or 50 m, to a typical modern turbine hub height ( $\sim 100$  m) introduces several assumptions (e.g. Hahmann et al., 2022), and thus considerable uncertainty is added when considering the magnitude of the wind speed. Thus, we avoid addressing the absolute value at a given grid point and focus on the spatial patterns of  $U_{50}$  based on the values at 10 m where all three reanalysis data are available.

### 2.3 The spectral correction method

110 The IEC standard requires that the 50-year return wind estimate is based on time series equivalent to a temporal resolution of 10-min. Thus, we cannot use the estimation of  $U_{50}$  directly from the 6-hourly CMIP6 data to refer to the IEC standard. The poor temporal sampling means that significant variability is missed compared to time series with a sampling rate every 10-min, which is essential for the estimation of the extreme wind (Larsén and Mann, 2006). When being presented as power spectrum  $S(f)$  as a function of frequency  $f$  (exemplified in Fig. 1), the original 6-hourly time series shows a fast decrease of energy from 115 about  $f = 1 \text{ day}^{-1}$  to very little energy at  $f = 2 \text{ day}^{-1}$ , and no energy for  $f > 2 \text{ day}^{-1}$ . We thus use the spectral correction method to fill the wind variability back to the CMIP6 time series. This method was developed by Larsén et al. (2012), in which it is assumed that that the once-per-year exceedance of the wind speed follows a Poisson process. At a threshold for the rate of once-per-year, such a distribution of the exceedance can be simplified as a Gaussian process. We use this method together with the Annual Maximum Method and the Gumbel distribution to calculate  $U_{50}$ .

120 The maximum wind that occurs once a year,  $\bar{U}_{\max}$ , is derived as a function of the zero- and second-order spectral moments  $m_0$  and  $m_2$ :

$$\bar{U}_{\max} = \bar{U} + \sqrt{m_0} \sqrt{2 \ln \left( \sqrt{\frac{m_2}{m_0}} T_0 \right)}, \quad (1)$$

where  $\bar{U}$  is the mean wind speed,  $T_0$  is the basis period of one year and  $m_i$  is the  $i$ th spectral moment defined by

$$m_i = 2 \int_0^{\infty} f^i S(f) df. \quad (2)$$

125 Equations 1 and 2 show that  $\bar{U}_{\max}$  is significantly affected by the values of  $S(f)$  at high frequencies through  $m_2$ . Thus, if we can correct the spectral tail, we can improve the calculation of  $\bar{U}_{\max}$ . We use a spectral model to estimate the tail of the distribution:

$$S(f) = a \cdot f^{-5/3}, \quad (3)$$

which is the mesoscale part of the expression from Larsén et al. (2013) for  $(1 \text{ day})^{-1} < f < 10^{-3} \text{ Hz}$ , where the value of the coefficient  $a$  can be derived from the spectrum of the model data. Exemplified for the time series in Fig. 1, we replace the 130

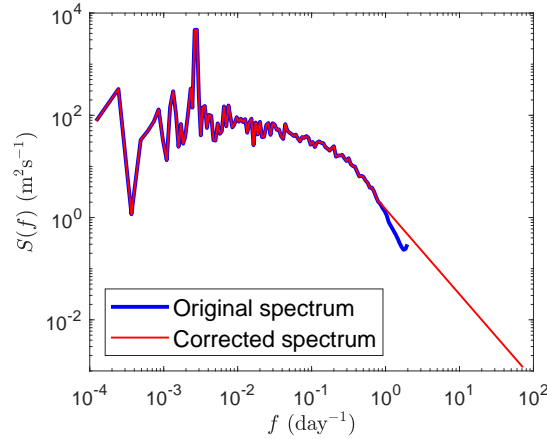


**Figure 1.** An example of the spectrum of the 6-hourly time series of wind speed at 100 m from the CNRM-CM6-1 model of historical period and the corrected spectrum to equivalent resolution of 10 min. The time series is from the location 56.7309°N, 9.84372°W

tapered-out spectrum in blue for  $f > 0.8 \text{ day}^{-1}$  with Eq. 3 for  $0.8 < f < 72 \text{ day}^{-1}$ , where  $72 \text{ day}^{-1}$  is the Nyquist frequency of a time series with a temporal resolution of 10-min. Then we apply Eq. 1 and 2 with both the original and corrected spectra to obtain  $\bar{U}_{\text{max,orig}}$  and  $\bar{U}_{\text{max,corr}}$ . The ratio of the two is used to correct the annual maximum values from the CMIP6 time series to the values equivalent to 10 min. The magnitude of the change from the spectral correction method depends on how smoothed  
135 the original time series is in comparison with what is expected of an observed 10-min time series. For the example shown in Fig. 1,  $U_{50} = 32.5 \text{ m s}^{-1}$  from the raw CMIP6 data and  $U_{50} = 42.8 \text{ m s}^{-1}$  after the spectral correction is applied.

### 3 Results

For each model grid point,  $U_{50}$  are calculated from the reanalysis data using the spectral correction method, and both  $U_{50}$  and the 95%-percentile ( $Q_{95}$ ) are calculated from the CMIP6 data for the his-Period and fut-Period. In the following, results of  
140  $U_{50}$  from the reanalysis data and CMIP6 of his-Period are presented in section 3.1.1 and 3.1.2, where the quality of the CMIP6 ensemble members is discussed. The CC impact on the extreme wind is analyzed in section 3.2.

#### 3.1 Extreme wind based on the historic period

##### 3.1.1 Reanalysis data

The 50-year wind  $U_{50}$  at 10 m from the CFSR, MERRA2 and ERA5 reanalysis data are shown in Fig. 2 for the his-Period.  
145 Over water, the spatial gradient in  $U_{50}$  is similar in the three data sets, with the highest values northwest of the British Islands and lowest in the northern Baltic Sea. Among the three, the CFSR and MERRA2-derived  $U_{50}$  are more similar with respect to the spatial patterns and magnitudes. The ERA5  $U_{50}$  at 10 m is on average systematically smaller. Over land, an obvious

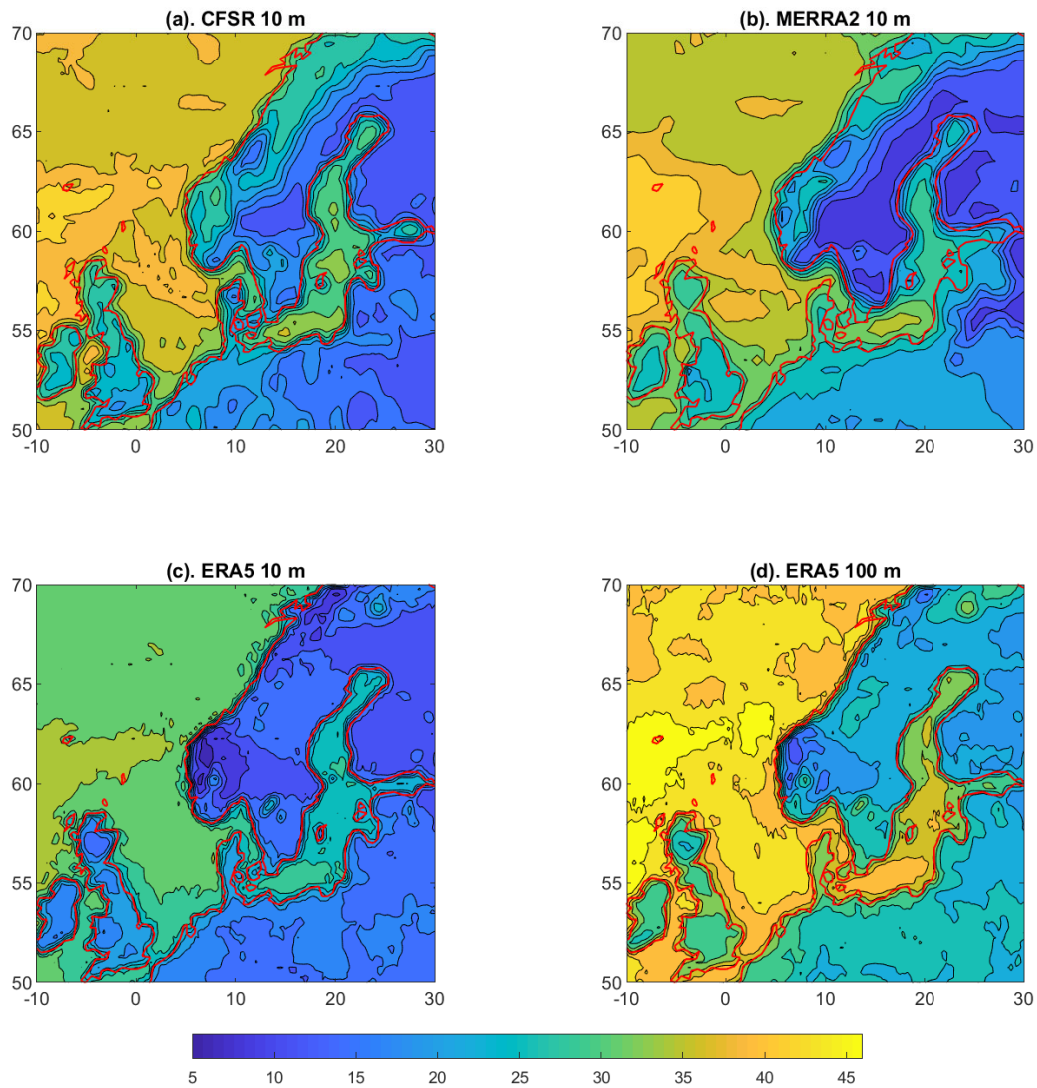


**Figure 2.** Spatial distribution of the spectral corrected 50-year wind for the his-Period derived from: (a) CFSR data at 10 m; (b) MERRA2 data at 10 m; (c) EAR5 data at 10 m; (d) ERA5 data at 100 m.



150 difference between ERA5 and the other two reanalysis data is the distribution over Norway and Sweden, where both CFSR and MERRA2 data suggest stronger extreme wind over western Norway and the smallest at approximate 61°N over Sweden, while the ERA5 data suggest lower extreme wind over western Norway and the smallest on the west coast at ~61°N. These patterns are suggested to be linked to extremely high surface roughness lengths in the MERRA2 over forest and the use of orographic drag in the ERA5 model (Dörenkämper et al., 2020). The spatial distribution is similar for the ERA5 data at 10 m and 100 m.

As mentioned in Section 1, a global atlas of  $U_{50}$  was made available in the GASP project at a spatial grid spacing of 275 m. We compare the spatial distribution of  $U_{50}$  at 100 m from ERA5 (Fig. 2d) and  $U_{50}$  at 100 m from the GASP project (see Fig. 5 in Larsén et al. (2022)). In the GASP data, the values of  $U_{50}$  at 100 m over water were derived using those at 10 m assuming a logarithmic wind profile law and a surface roughness length parameterization from the wave model SWAN (Larsén et al., 2022); over land, the values from the CFSR reanalysis data were downscaled using microscale modeling, see also Larsén et al. (2022). The large scale pattern of  $U_{50}$  from GASP is consistent with what we observed here. The values over land vary by 20–40 m s<sup>-1</sup> and those over water from about 25 to 55 m s<sup>-1</sup>. Offshore, the values at 100 m are comparable to the ones in Fig. 2d, namely ERA5 data at 100 m.

Due to the differences in the various reanalysis data it is difficult to conclude which one of them is the best without a systematic validation with measurements. Thus, we focus on the characteristics of the wind distribution that are shared by these reanalysis data and use them to discuss the quality of the CMIP6 data for his-Period. We use the following wind characteristics that are present in the three reanalyses: (a) The 50-year wind at 100 m  $U_{50,100m}$  ranges between about 5 and 55 m s<sup>-1</sup>; (b) Stronger winds over the North Sea than over the Baltic Sea; (c) Strongest  $U_{50}$  in the northern North Sea; (d) Clear land-sea difference: stronger winds over water than over land. Using these four characteristics of  $U_{50}$  we will create an index, defined as the large-scale score (with 0 meaning “not matching” and 1 meaning “matching”), and use it for data analysis of the CMIP6 model outputs (Table 2).

### 3.1.2 CMIP6 data

170 We use the same procedure as used for the reanalysis data, e.g., through the spectral correction method, Annual Maximum Method and the Gumbel distribution fit, to calculate  $U_{50}$  for the 18 CMIP6 models at three heights 50, 100 and 200 m. Fig. 3 shows the spatial distribution of  $U_{50}$  from the 18 models at 100 m.

We use the four characteristics, (a)–(d), as described at the end of section 3.1.1 to give a score 0 or 1 to the 18 models. The results of this scoring are summarized in Table 2. The four criteria are generous, and therefore the scoring is qualitative. In the end, we have 6 models with highest score 4 (models 1, 5, 6, 9, 10, 18) and 3 models with lowest score 2 (models 8, 11, 14). To explore the sensitivity of the collection of model data, we perform the data analysis to different grouping of models. The groups are defined as follows: Group-I includes all 18 models, Group-II includes all models of a score of 4 (6 models), and Group-III with models with a score of 3 and 4 (15 models). The three groups are also shown in Table 2.

180 We validate the calculations of  $U_{50}$  at 100 m from the CMIP6 data with those from measurements at the three FINO masts from Larsén et al. (2019). At FINO 1, 2 and 3, the 50-year wind is 41.1, 35.3 and 40.2 m s<sup>-1</sup>, respectively, using Annual/Periodic Maximum Method ( $U_{50,obs,PM}$ ). The corresponding values are 41.2, 38.2 and 43.0 m s<sup>-1</sup>, respectively, using



**Table 2.** Score of the large-scale extreme wind for the his-Period for the 18 CMIP6 models (labeled as defined in Table 1) using the four wind characteristics defined in section 3.1.2. Also shown are the three model groups that include (I) all models; (II) models with total score of 4; (III) models with score 3 or 4.

No.	Model	a	b	c	d	Total	Group-I	Group-II	Group-III
1	ACCESS-CM2	1	1	1	1	4	*	*	*
2	CanESM5	1	1	1	0	3	*		*
3	CESM2	1	1	1	0	3	*		*
4	CMCC-CM2-SR5	1	1	1	0	3	*		*
5	CNRM-CM6-1	1	1	1	1	4	*	*	*
6	CNRM-ESM2-1	1	1	1	1	4	*	*	*
7	HadGEM3-GC31-LL	1	1	1	0	3	*		*
8	HadGEM3-GC31-MM	1	1	0	0	2	*		
9	IPSL-CM6A-LR	1	1	1	1	4	*	*	*
10	MIROC6	1	1	1	1	4	*	*	*
11	MIROC-ES2L	1	1	0	0	2	*		
12	MPI-ESM1-2-HR	1	1	1	0	3	*		*
13	MPI-ESM1-2-LR	1	1	1	0	3	*		*
14	MRI-ESM2-0	1	1	0	0	2	*		
15	NESM3	1	1	1	0	3	*		*
16	NorESM2-LM	1	1	1	0	3	*		*
17	NorESM2-MM	1	1	1	0	3	*		*
18	UKESM1-0-LL	1	1	1	1	4	*	*	*

the Peak Over Threshold method ( $U_{50,obs,POT}$ ). Please refer to Larsén et al. (2019) for the measurement details and the theories and algorithms used in the PMM and POT methods. Note that the data periods and lengths from the FINO sites are shorter and different from the CMIP6 historical data; this can bring uncertainties to the comparison. To show the uncertainties related to limited time series, Larsén et al. (2019) calculates the  $U_{50}$  using both the PMM and POT methods.

Figure 4 presents the difference of the estimates of  $U_{50}$  in percentage between the measured and modeled values for the three FINO sites. Even though some CMIP6 models provide more consistent large scale patterns, their performance at the three offshore sites are not necessarily best (e.g. model 10). Models with lowest large-scale scores as in Table 2 (model 11 and 14) also show poor performance at the three sites, while the performance of model 8, which as a large-scale score of 2, has little bias.

### 3.2 Climate change impact on the extreme wind

The effect of CC on the extreme wind is estimated through the differences in the various extreme wind variables previously defined between the future period (fut-Period) and the historical period (his-Period). This includes the mean and relative

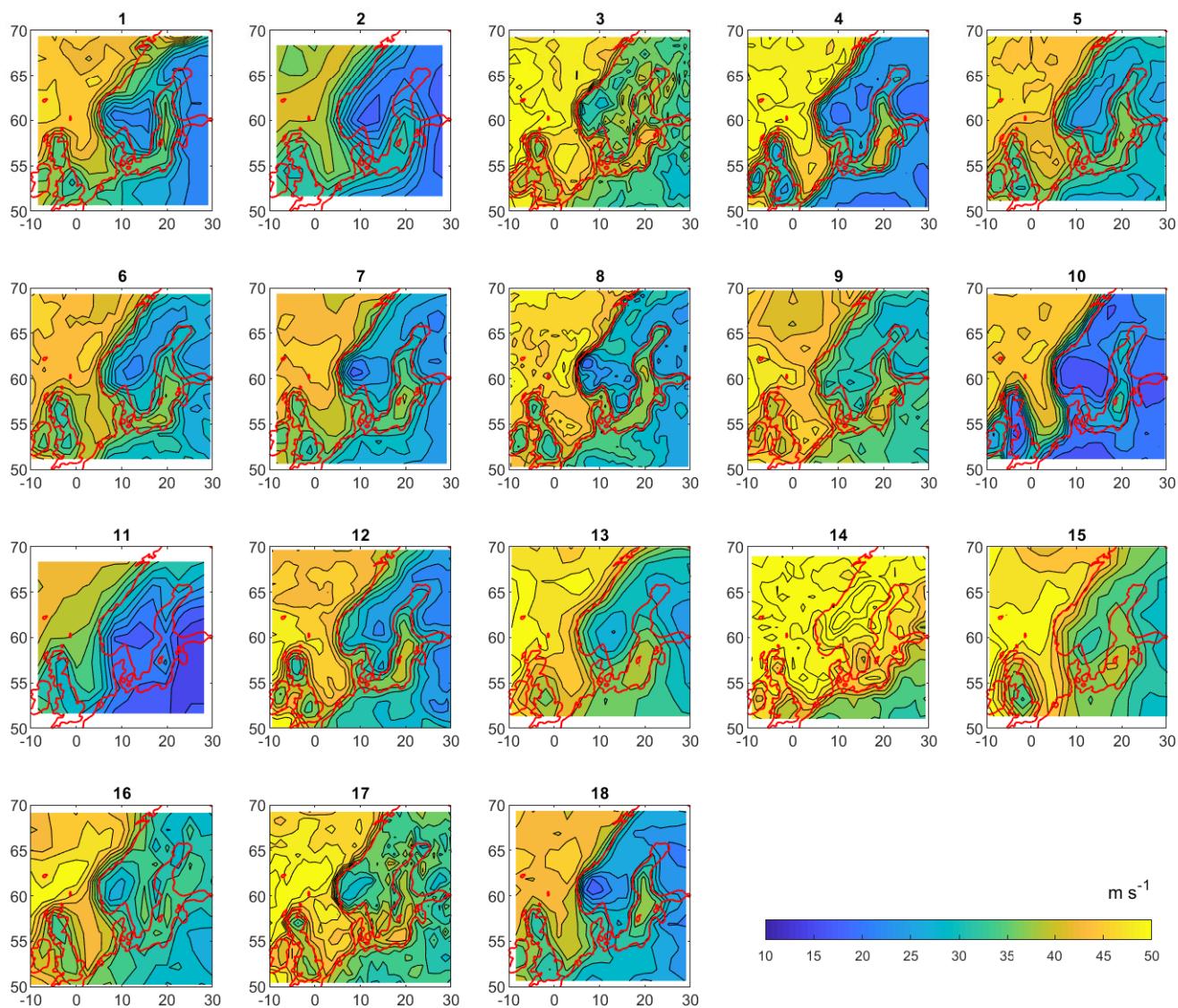


**Figure 3.** The 50-year wind at 100 m for the 18 CMIP6 models for the his-period,  $U_{50,\text{his}}$ , estimated using the spectral correction. The model's labels follow those defined in Table 1.

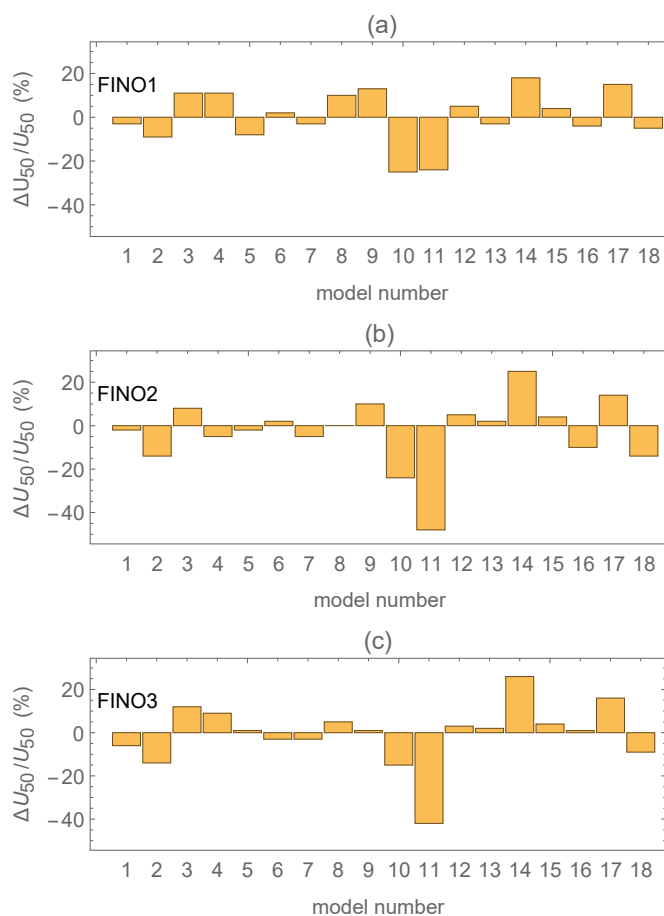


**Figure 4.** Comparison of  $U_{50}$  at 100 m at the three measurement sites: (a) FINO1, (b) FINO2 and (c) FINO3, between the observed value and that of the 18 CMIP6 models (labeled as defined in Table 1) for the his-Period. The values are the mean value of  $\Delta U_{50,PMM}/U_{50,obs,PMM}$  and  $\Delta U_{50,POT}/U_{50,obs,POT}$ , in %, where  $\Delta U_{50,PMM} = U_{50,obs,PMM} - U_{50,CMIP6}$  and  $\Delta U_{50,POT} = U_{50,obs,POT} - U_{50,CMIP6}$ .  $U_{50,obs,PMM}$  and  $U_{50,obs,POT}$  are from Larsén et al. (2019).



195 differences in  $U_{50}$  and the 95th percentile of the wind speed,  $Q_{95}$  from the 18 models at each grid point (Fig. 5 and 6). A description of the model spread of the differences at each grid point is shown in Fig. 7 and the summary statistics over the entire domain are shown in Table 3.

We first explore the effect of CC on  $U_{50}$ . We compute the difference between the fut-Period ( $U_{50,\text{fut}}$ ) and the his-Period ( $U_{50,\text{his}}$ ) for each model:  $\Delta U_{50,i} = U_{50,i,\text{fut}} - U_{50,i,\text{his}}$ , with  $i = 1, \dots, 18$ . As the grid spacing of the 18 models is different, we interpolate all models to the reference grid from model 5 through a nearest-neighbor interpolation. To assess the sensitivity of using different models, the comparison is done for the three groupings of models earlier defined as Group-I (all 18 models), II (6 models with large-scale score 4) and III (15 models with large-scale score 3 and 4), see Table 2. The results for 100 m are shown in Fig. 5 for absolute (left column) and relative ( $r = \Delta U_{50}/U_{50,\text{his}}$ ; right column) differences. A similar calculation for the second variable, the 95th percentile of the wind speed 100 m, is shown in Fig. 6.

To obtain an overview of how robust the changes are across the CMIP6 models, we summarize the agreement in results of the relative differences in  $\Delta U_{50}$  and  $\Delta Q_{95}$ . Five ranges of  $r$  are used to examine the agreement among models:  $r > 5\%$  (significant increase; SI),  $2\% < r \leq 5\%$  (medium increase; MI),  $-2\% < r \leq 2\%$  no obvious change (neutral),  $-5\% < r \leq -2\%$  (medium decrease; MD) and  $r \leq -5\%$  (significant decrease; SD). This classification is done for each model and each grid point. Note that the definition of significance level is arbitrary and only valid for the analysis in this paper. In Fig. 7 we show the  $r$  range (SI, MI, etc) supported by the largest number of models. The three rows are for model Group-I, II and III, respectively; the two columns are for  $\Delta U_{50}$  (left) and  $\Delta Q_{95}$  (right).

Figures 5 and 6 show high agreement between the spatial patterns of  $\Delta U_{50}$  and  $\Delta Q_{95}$ . At first glance, the CMIP6 models prediction for the future suggest an increase in the extreme wind over the west part of the domain (including the UK, Denmark and parts of Germany) except for the northwestern Atlantic, where the ensemble mean show a decrease in extreme wind. The results also indicate that CC could lead to reduced extreme wind over most of the eastern part of the model domain, including Sweden, Finland, parts of Poland and middle part of the Baltic Sea for the near future (2020–2049) based on the SSP585 high emission scenario. These features are present in all model groups (group-I, II and III), even though there are some differences between them. Table 3 summarizes the statistics of  $\Delta U_{50}$  and  $\Delta Q_{95}$  for the three CMIP6 model groupings. The statistics for Group-I are rather similar to Group-III, while Group-II, which has only 6 models, shows slightly larger differences but consistent results. The overall trend over the whole domain suggests slightly weaker extreme wind in the fut-Period averaged over all CMIP6 models. For the majority of grid points in the model domain, most models indicate no obvious change (“neutral”  $\sim 35 - 52\%$  depending on the ensemble group), and many grid points show significant increase or significant decrease. From Fig. 7, the CMIP6 models suggest the largest chance of reduced extreme winds in the near future mostly over land in the middle part of Norway and Sweden and part of Poland. Over the Baltic Sea, the CMIP6 ensemble suggests the largest possibility of reduced extreme wind in the north, but of increased extreme wind in the south. For grid points over the North Sea, the CMIP6 ensemble suggests mostly increase or unchanged in extreme winds. The pattern elsewhere is unclear.

To discuss the relevance and importance of the CC effect on the extreme winds, we relate the extreme wind change to the turbine class as defined in the IEC standard (IEC, 2019). Turbine classes I, II, III and TC (for most severe storms such as tropical cyclones) are defined based on the threshold 10-min values of  $U_{50}$  at hub height (Table 4). To quantify the CC impact

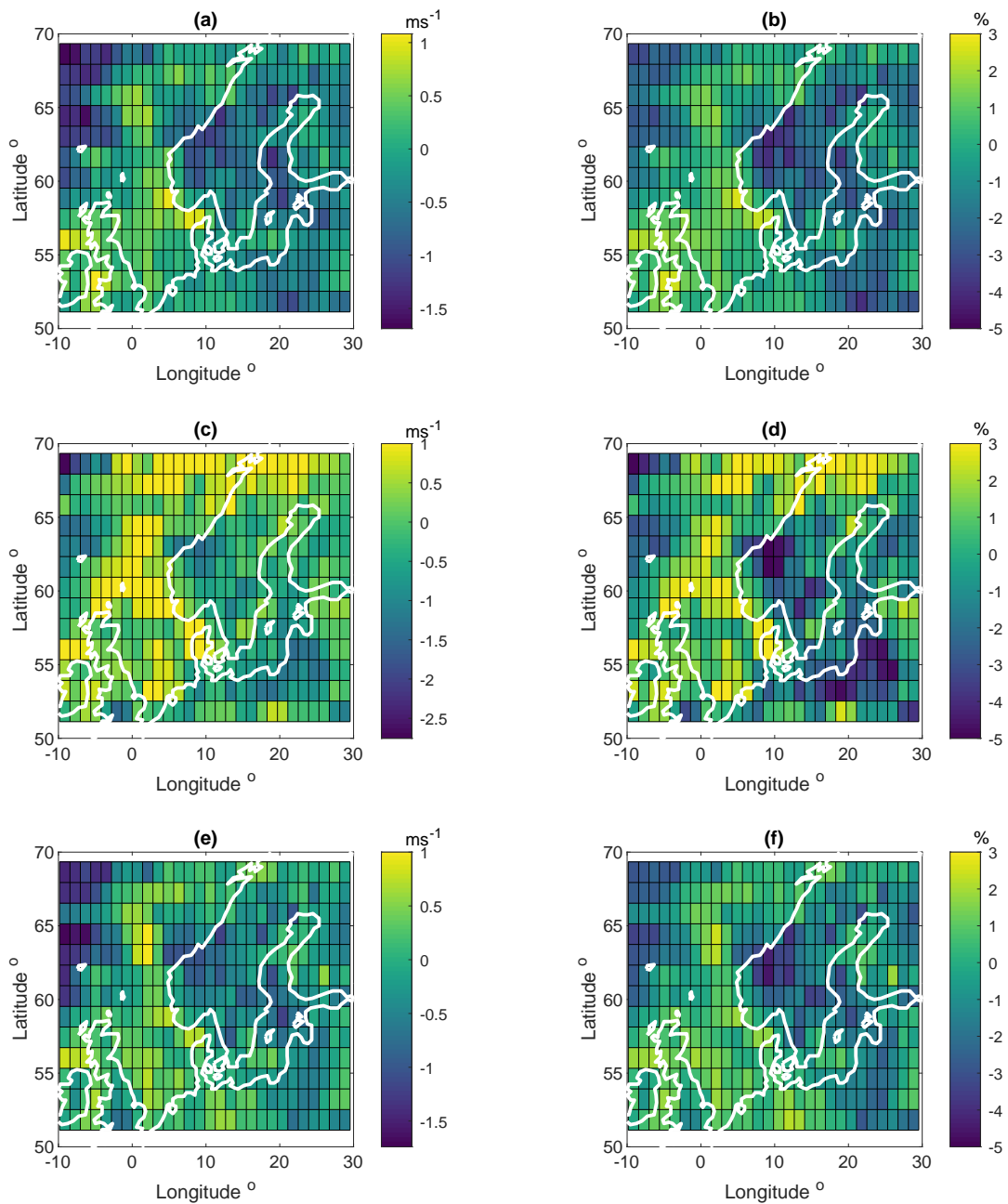


**Figure 5.** Spatial distribution of model mean difference  $\Delta U_{50}$  (left column) and relative mean difference  $(\Delta U_{50}/U_{50, his})$  (right column) between the his- and fut-Periods, for model Group-I (a and b), Group-II (c and d); and Group-III (e and f).

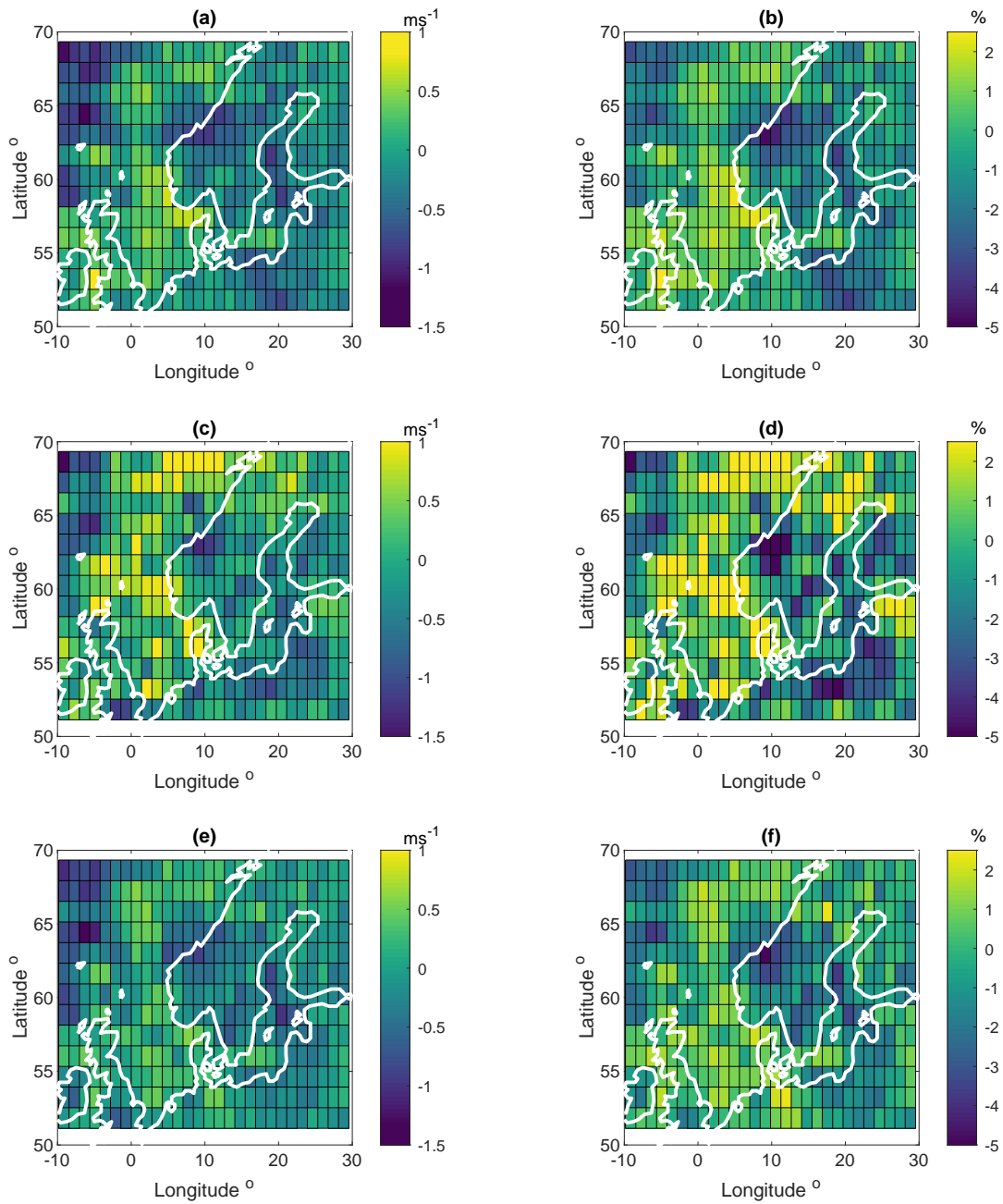


**Figure 6.** Same as Fig. 5, but for the 95% quantile of the wind speed at 100 m.

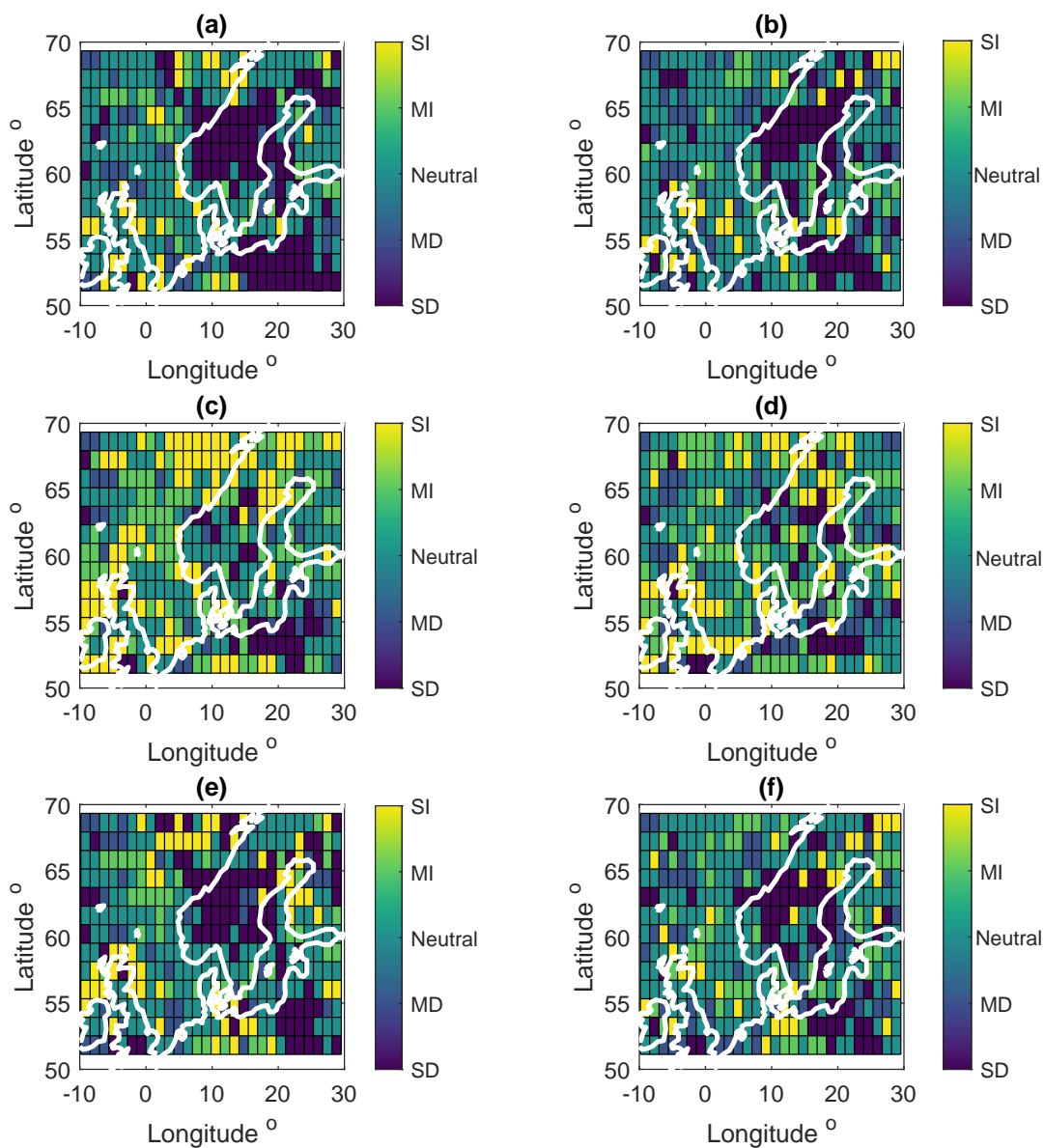


**Figure 7.** Range (SI–significant increase, MI–medium increase, neutral–no obvious change, MD–medium decrease, SD–significant decrease, see text) in relative change in  $\Delta U_{50}$  (left column) and  $\Delta Q_{95}$  (right column) at 100 m supported by the largest number of CMIP6 models in Group-I (a and b), Group-II (c and d), and Group-III (e and f).



**Table 3.** Summary of the statistics of change in the extreme wind  $\Delta U_{50}$  at 100 m (Fig. 5) and  $\Delta Q_{95}$  (Fig. 6) over the entire domain.

Variables	Statistics	Grouping of CMIP6 models		
		Group-I (all models)	Group-II (models 1, 5, 6, 9, 10, 18)	Group-III (models 1–7, 9, 10, 12, 13, 15–18)
$U_{50}$	mean $\pm \sigma$ ( $\text{ms}^{-1}$ )	$-0.23 \pm 0.51$	$0.008 \pm 0.78$	$-0.17 \pm 0.50$
	min, median, max ( $\text{ms}^{-1}$ )	-1.69, -0.20, 1.08	-2.76, -0.01, 2.23	-1.74, -0.12, 1.13
	SI area (%)	24.4	8.4	20.7
	MI area (%)	12.6	8.4	12.3
	neutral area (%)	44.1	34.7	40.9
	MD area (%)	8.1	22.2	10.6
	SD area (%)	10.8	26.4	15.5
$Q_{95}$	mean $\pm \sigma$ ( $\text{ms}^{-1}$ )	$-0.15 \pm 0.35$	$-0.03 \pm 0.54$	$-0.12 \pm 0.36$
	min, median, max ( $\text{ms}^{-1}$ )	-1.13, -0.14, 1.00	-1.63, -0.06, 1.55	-1.27, -0.12, 0.99
	SI area (%)	19.5	8.6	17.5
	MI area (%)	13.3	12.1	13.1
	neutral area (%)	50.0	37.7	45.8
	MD area (%)	9.4	22.0	13.8
	SD area (%)	7.9	19.7	9.9

on the possible change in turbine class, we assign  $\text{TCL}=1-4$  to the four classes as in the IEC standard plus an additional class,  $\text{TCL}=5$ , for  $U_{50} > 57 \text{ m s}^{-1}$ . The corresponding changes in TLC class are calculated for each CMIP6 model and each grid point. The analysis was done for the three model groupings (Group-I, II, and III) to assess the robustness of the results across CMIP6 models. For Groups I, II and III, there is no change of turbine class in the near future at any evaluated grid point. Figure 8 shows an example for Group-II. According to the six models in Group-II, the optimal turbine class in most areas will not change in the near future due to CC. While some areas show a change in optimal TCL, the areas are not necessarily consistent in all models. For instance, model 1 (ACCESS-CM2) suggests a lower turbine class in the near future over the water in the north, and a higher turbine class in part of the southern North Sea; model 9 has contradicting suggestions. Model 5 suggests higher turbine classes in the coast areas of Norway, Finland, Denmark, the Baltic Sea and south of the North Sea; model 18 also has contradicting suggestions (except for the most northern part of the UK). These results suggest that in this region there is no conclusive trend in the change in the extreme winds that will provoke a shift towards a need for higher turbine classes in the future. A change towards a higher turbine class would make wind energy development more expensive in the future. The same calculations was done at 50 m and 200 m and the conclusions remain the same.

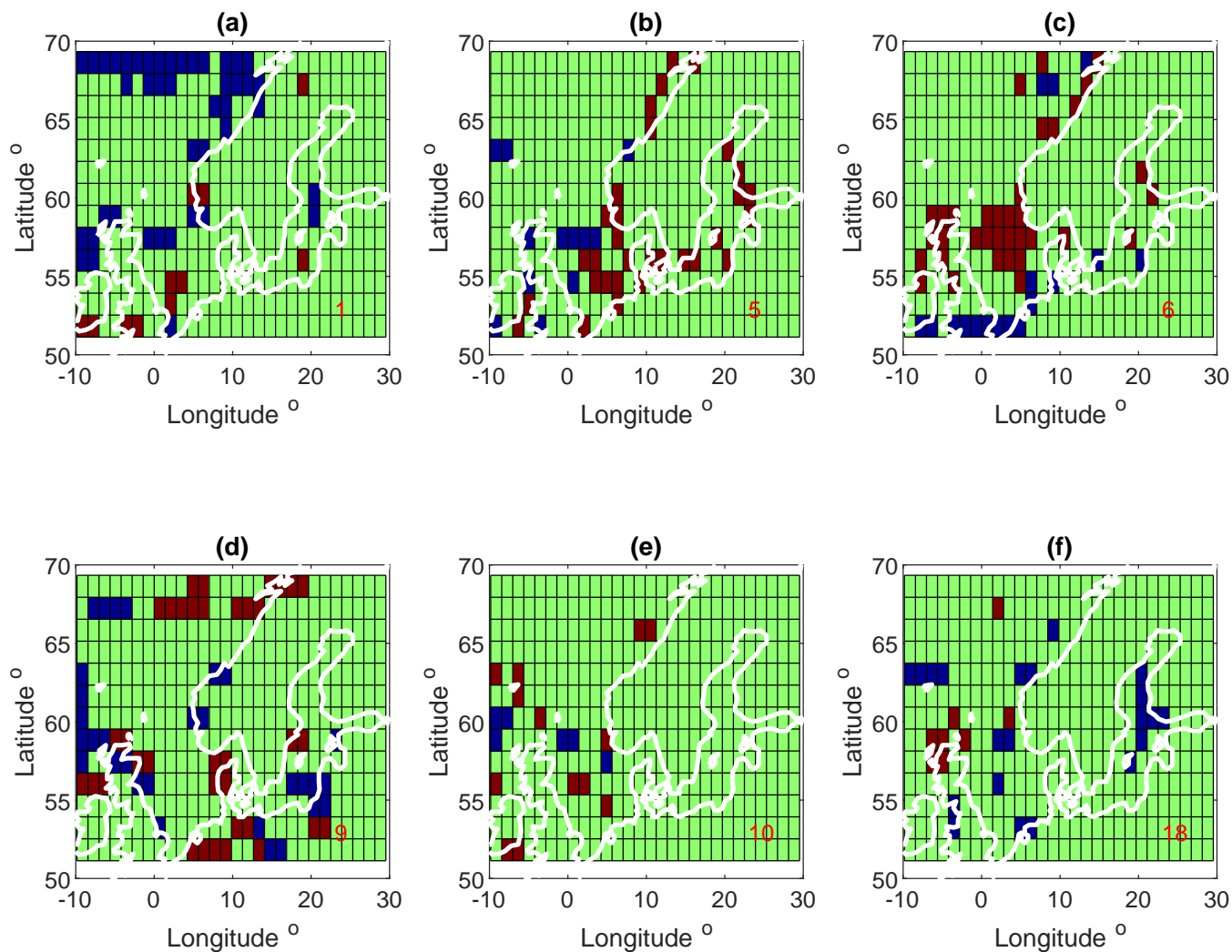


**Figure 8.** Change in the future TCL for 100 m in the six models in Group-II: (a) ACCESS-CM2; (b) CNRM-CM6-1; (c) CNRM-ESM2-1; (d) IPSL-CM6A-LR; (e) MIROC6; (f) UKESM1-0-LL. The colors indicate: one class stronger (red), one class weaker (blue) and no changes (green) .



**Table 4.** Turbine classes (TCL) with corresponding extreme wind ranges, and the assigned index.

Turbine Class	$U_{50}$ range, $\text{m s}^{-1}$	TCL
I	(0, 37.5]	1
II	(37.5, 42.5]	2
III	(42.5, 50]	3
TC	(50, 57]	4
	[57, $\infty$ )	5

#### 4 Discussion

In this study we investigated the climate change effect on the 50-year wind, which is one of the key design parameters for wind turbines. We used outputs from 18 CMIP6 models, which is about half of all models submitted to CMIP6. We also chose to use the high-emission SSP585 scenario, following Hahmann et al. (2022). Such a selection faces the question whether this collection of models is sufficient for drawing robust conclusions. The models were chosen because of the availability of a number of variables needed for deriving the wind speeds at turbine hub heights from the values at model levels (Hahmann et al., 2022). With this limitation, we note that the analysis and conclusions drawn here may be updated in the future when more relevant data are made available by the community. At the same time, it is worth finding out what the 18 models suggest regarding the CC effect on the extreme wind, when being compared with previous studies using other data sources.

A common challenge in analyzing ensemble data is to separate the “signal” from the “noise”, as signals can be buried in the group of models (e.g. Smith et al., 2020; Outten and Esau, 2013). Smith et al. (2020) pointed it out: “Quantifying signals and uncertainties in climate models is essential for the detection, attribution, prediction and projection of climate change”. Even within different reanalysis products that should be representative of the historic data, there are already significant discrepancies in their estimations of extreme winds. Our approach for “extracting signals” of CC include the comparison of the large scale distribution pattern of the extreme wind between the CMIP6 model data that are consistently presented by the three reanalysis data, and the average of the increase and decrease in the extreme wind parameters in the model ensemble. It must be noted that the chosen analysis approach is based on the assumption that consistent behaviour between the CMIP6 models is an indicator for higher probability of occurrence under the given scenario (e.g. Christensen et al., 2019). This assumption is commonly used in the IPCC assessment report (IPCC, 2021). There are systematic and consistent patterns for increased and decreased extreme winds that can be identified in certain regions, for both  $U_{50}$  and  $Q_{95}$ , even though we are using different groups of data from the 18 CMIP6 models.

Among the many studies on climate change impact, the impact on extreme wind conditions is one of those that does not lead to a clear conclusion. The following patterns have been summarized in earlier studies using different model outputs and scenarios: (a) Overall increasing extreme wind parameters in Northern Europe (e.g. Donat et al., 2011; Pryor et al., 2012; Christensen et al., 2022); (b) Increase over the Baltic Sea (e.g. NIKULIN et al., 2011; Christensen et al., 2022); (c) Small insignificant increase with large spread in the southern part of the Baltic Sea. Christensen et al. (2022) found from 72 EURO-



CORDEX RCP8.5 simulations very little agreement on even the sign of wind speed change. With the current study, some key statistics can be summarized (see e.g. Table 3), including: over the entire study domain, an overall decrease in  $U_{50}$  and  $Q_{95}$ ; the largest model group (about 40%) suggests no considerable change, 20% of models suggests significant increase and a slightly smaller number of models suggests significant decrease. Geographically, quite a large area of the North Sea corresponds to an average increase, and most part of the Baltic Sea and the Scandinavian Peninsula corresponds to an average decrease. Most analyses here also support a medium increase in southern part of the Baltic Sea. While the analysis has also shown some degree of sensitivity regarding the models used, the overall conclusions are consistent (Fig. 5, 6 and 7).

To assess the importance of CC on the extreme wind (and thus on wind turbine siting), we relate the results to the IEC standards and discuss how it affects the design criteria for turbines. There is a high diversity between models on the general analysis of extreme wind and there is no consensus anywhere in the studied domain regarding if it will be more expensive or cheaper in the future to install wind turbines (Fig. 8). Most models suggest no change in turbine class over most grid points.

This study only downscaled the CMIP6 data in temporal domain using the spectral correction method, so that the calculated extreme wind of the time series matches that of a 10-min time series (requirement from the IEC standard). The spatial details are thus not resolved. For the 18 CMIP6 models, the quality of the extreme wind simulation, which is assessed through the comparison of extreme wind distribution pattern with reanalysis data and comparison with values from measurements at three offshore sites, does not show any dependence on the spatial resolution of the CMIP6 data. These data have a spatial resolution ranging from about 80 km to a couple of hundreds of kilometers. This will of course introduce uncertainties and thus we can only discuss CC on a large scale.

## 5 Conclusions

Eighteen CMIP6 ensemble members are used to assess climate change impact on extreme wind over Northern Europe. There is a large diversity of suggestions of impacts between the model members. The analysis shows an overall increase in the extreme winds in the North Sea and southern part of the Baltic Sea, but a decrease in the Scandinavian Peninsula and most part of the Baltic Sea. However such a climate change as projected by the CMIP6 data does not suggest more expensive or cheaper turbines to be used in the area.

*Code and data availability.* We provide a few examples of the Python code used to search, extract and interpolate and locally write the winds in the CMIP6 data. The code resides in <https://github.com/ahahmann/future-wind/>.

*Author contributions.* XL outlined and wrote the paper and did analysis; MI did calculations and analysis; ÁH did calculations; AH extracted the CMIP6 data. All authors participated in writing and editing of the manuscript.



*Competing interests.* The authors declare no competing interests.

*Acknowledgements.* This study is supported by the GASPOC project (EUDP 64020-1043).

The ERA5 data were downloaded from ECWMF and Copernicus Climate Change Service Climate Data Store. MERRA2 data are downloaded from the Distributed Active Archive Center (GSFC DAAC), DOI: 10.5067/VJAFPLI1CSIV. FINO 1, 2, and 3 were supplied by  
300 German Federal Maritime And Hydrographic Agency (BSH). CFSR data have been retrieved from the Research Data Archive of the National Center for Atmospheric Research (<https://doi.org/10.5065/D6513W89>) The CMIP6 multi-model ensemble data were downloaded through the distributed data archive developed and operated by the Earth System Grid Federation (ESGF; <https://esgf.llnl.gov/>).



## References

- ENSEMBLES, <https://ensembles-eu.metoffice.com/>.
- 305 PRUDENCE, <https://www.wcrp-climate.org/modelling-wgcm-mip-catalogue/modelling-wgcm-mips-2/288-modelling-wgcm-catalogue-prudence>.
- Bastine, D., Larsén, X., Witha, B., Dörenkämper, M., and Gotschall, J.: Extreme winds in the new European Wind atlas, *Journal of Physics: Conf. Series*, 1102, 012006, 2018.
- Beniston, M., Stephenson, D. B., Christensen, O. B., Ferro, C. A. T., Frei, C., Goyette, S., Halsnaes, K., Holt, T., Jylha, K., Kofli, B.,  
310 Palutikof, J., Scholl, R., Semmler, T., and Woth, K.: Future extreme events in European climate: an exploration of regional climate model projections, *Climatic Change* 81, 2007.
- Boucher, O., Servonnat, J., Albright, A. L., Aumont, O., Balkanski, Y., Bastrikov, V., Bekki, S., Bonnet, R., Bony, S., Bopp, L., Braconnot, P., Brockmann, P., Cadule, P., Caubel, A., Cheruy, F., Codron, F., Cozic, A., Cugnet, D., D'Andrea, F., Davini, P., de Lavergne, C., Denvil, S., Deshayes, J., Devilliers, M., Ducharne, A., Dufresne, J.-L., Dupont, E., Éthé, C., Fairhead, L., Falletti, L., Flavoni, S.,  
315 Foujols, M.-A., Gardoll, S., Gastineau, G., Ghattas, J., Grandpeix, J.-Y., Guenet, B., Guez, Lionel, E., Guilyardi, E., Guimberteau, M., Hauglustaine, D., Hourdin, F., Idelkadi, A., Joussaume, S., Kageyama, M., Khodri, M., Krinner, G., Lebas, N., Levvasseur, G., Lévy, C., Li, L., Lott, F., Lurton, T., Luysaert, S., Madec, G., Madeleine, J.-B., Maignan, F., Marchand, M., Marti, O., Mellul, L., Meurdesoif, Y., Mignot, J., Musat, I., Ottlé, C., Peylin, P., Planton, Y., Polcher, J., Rio, C., Rochetin, N., Rousset, C., Sepulchre, P., Sima, A., Swingedouw, D., Thiéblemont, R., Traore, A. K., Vancoppenolle, M., Vial, J., Vialard, J., Viovy, N., and Vuichard, N.: Presentation and Evaluation of the IPSL-CM6A-LR Climate Model, *Journal of Advances in Modeling Earth Systems*, 12, e2019MS002010,  
320 <https://doi.org/https://doi.org/10.1029/2019MS002010>, e2019MS002010 10.1029/2019MS002010, 2020.
- Brasseur, G. and Carlson, D.: Future directions for the World Climate Research Programme, *EOS*, 96,  
<https://doi.org/10.1029/2015EO033577>, 2015.
- Cherchi, A., Fogli, P. G., Lovato, T., Peano, D., Iovino, D., Gualdi, S., Masina, S., Scoccimarro, E., Materia, S., Bellucci, A., and Navarra,  
325 A.: Global Mean Climate and Main Patterns of Variability in the CMCC-CM2 Coupled Model, *Journal of Advances in Modeling Earth Systems*, 11, 185–209, <https://doi.org/https://doi.org/10.1029/2018MS001369>, 2019.
- Christensen, J., Larsen, M., and Christensen, O. e. a.: Robustness of European climate projections from dynamical downscaling, *Clim Dyn*, 53, 4857–4869, <https://doi.org/https://doi.org/10.1007/s00382-019-04831-z>, 2019.
- Christensen, O. B., Kjellström, E., Dieterich, C., Gröger, M., and Meier, H. E. M.: Atmospheric regional climate projections for the Baltic  
330 Sea region until 2100, *Earth System Dynamics*, 13, 133–157, <https://doi.org/10.5194/esd-13-133-2022>, 2022.
- Clausen, N.-E., Larsén, X., Pryor, S., and Drews, M.: Wind power, pp. 147–160, no. 502 in TemaNord, Nordic Council of Ministers, 2012.
- Danabasoglu, G., Lamarque, J.-F., Bacmeister, J., Bailey, D. A., DuVivier, A. K., Edwards, J., Emmons, L. K., Fasullo, J., Garcia, R., Gattelman, A., Hannay, C., Holland, M. M., Large, W. G., Lauritzen, P. H., Lawrence, D. M., Lenaerts, J. T. M., Lindsay, K., Lipscomb, W. H., Mills, M. J., Neale, R., Oleson, K. W., Otto-Bliesner, B., Phillips, A. S., Sacks, W., Tilmes, S., van Kampenhout, L., Vertenstein, M., Bertini, A., Dennis, J., Deser, C., Fischer, C., Fox-Kemper, B., Kay, J. E., Kinnison, D., Kushner, P. J., Larson, V. E., Long, M. C.,  
335 Mickelson, S., Moore, J. K., Nienhouse, E., Polvani, L., Rasch, P. J., and Strand, W. G.: The Community Earth System Model Version 2 (CESM2), *Journal of Advances in Modeling Earth Systems*, 12, e2019MS001916, <https://doi.org/https://doi.org/10.1029/2019MS001916>, e2019MS001916 2019MS001916, 2020.



- Della-Marta, P., Mathis, H., Frei, C., Liniger, M., Kleinn, J., and Appenzeller, C.: The return period of wind storms over Europe, *International Journal of Climatology*, 29, 437 – 459, <https://doi.org/10.1002/joc.1794>, 2009.
- Donat, M. G., Leckebusch, G. C., Wild, S., and Ulbrich, U.: Future changes in European winter storm losses and extreme wind speeds inferred from GCM and RCM multi-model simulations, *Natural Hazards and Earth System Sciences*, 11, 1351–1370, <https://doi.org/10.5194/nhess-11-1351-2011>, 2011.
- Dörenkämper, M., Olsen, B. T., Witha, B., Hahmann, A. N., Davis, N. N., Barcons, J., Ezber, Y., Garcíá-Bustamante, E., Fidel González-Rouco, J., Navarro, J., Sastre-Marugán, M., Sile, T., Trei, W., Žagar, M., Badger, J., Gottschall, J., Rodrigo, J. S., and Mann, J.: The Making of the New European Wind Atlas - Part 2: Production and evaluation, *Geoscientific Model Development*, 13, 5079–5102, <https://doi.org/10.5194/gmd-13-5079-2020>, 2020.
- Eyring, V., Bony, S., Meehl, G. A., Senior, C. A., Stevens, B., Stouffer, R. J., and Taylor, K. E.: Overview of the Coupled Model Intercomparison Project Phase 6 (CMIP6) experimental design and organization, *Geoscientific Model Development*, 9, 1937–1958, <https://doi.org/10.5194/gmd-9-1937-2016>, 2016.
- Gelaro, R., McCarty, W., Suárez, M. J., Todling, R., Molod, A., Takacs, L., Randles, C. A., Darmenov, A., Bosilovich, M. G., Reichle, R., Wargan, K., Coy, L., Cullather, R., Draper, C., Akella, S., Buchard, V., Conaty, A., da Silva, A. M., Gu, W., Kim, G.-K., Koster, R., Lucchesi, R., Merkova, D., Nielsen, J. E., Partyka, G., Pawson, S., Putman, W., Rienecker, M., Schubert, S. D., Sienkiewicz, M., and Zhao, B.: The Modern-Era Retrospective Analysis for Research and Applications, Version 2 (MERRA-2), *Journal of Climate*, 30, 5419–5454, <https://doi.org/10.1175/jcli-d-16-0758.1>, 2017.
- Giorgi, F. and Gutowski, W. J.: Regional Dynamical Downscaling and the CORDEX Initiative, *Annu. Rev. Environ. Resour.*, 40, 467–490, 2015.
- GWEC: Global Wind Report 2022, [https://gwec.net/wp-content/uploads/2022/04/Annual-Wind-Report-2022\\_screen\\_final\\_April.pdf](https://gwec.net/wp-content/uploads/2022/04/Annual-Wind-Report-2022_screen_final_April.pdf), 2022.
- Hahmann, A. N., García-Santiago, O., and Peña, A.: Current and future wind energy resources in the North Sea according to CMIP6, *Wind Energy Science Discussions*, 2022, 1–32, <https://doi.org/10.5194/wes-2022-52>, 2022.
- Hajima, T., Watanabe, M., Yamamoto, A., Tatebe, H., Noguchi, M. A., Abe, M., Ohgaito, R., Ito, A., Yamazaki, D., Okajima, H., Ito, A., Takata, K., Ogochi, K., Watanabe, S., and Kawamiya, M.: Development of the MIROC-ES2L Earth system model and the evaluation of biogeochemical processes and feedbacks, *Geoscientific Model Development*, 13, 2197–2244, <https://doi.org/10.5194/gmd-13-2197-2020>, 2020.
- Hansen, B. O., Larsén, X. G., Kelly, M., Rathmann, O. S., Berg, J., Bechmann, A., Sempreviva, A. M., and Jørgensen, H. E.: Extreme wind calculation applying spectral correction method - test and validation, Tech. rep., Wind Energy Department, Technical University of Denmark, DTU Wind Energy E-0098, 2016.
- Hersbach, H., Bell, B., Berrisford, P., Hirahara, S., Horányi, A., Muñoz-Sabater, J., Nicolas, J., Peubey, C., Radu, R., Schepers, D., Simmons, A., Soci, C., Abdalla, S., Abellan, X., Balsamo, G., Bechtold, P., Biavati, G., Bidlot, J., Bonavita, M., Chiara, G., Dahlgren, P., Dee, D., Diamantakis, M., Dragani, R., Flemming, J., Forbes, R., Fuentes, M., Geer, A., Haimberger, L., Healy, S., Hogan, R. J., Hólm, E., Janisková, M., Keeley, S., Laloyaux, P., Lopez, P., Lupu, C., Radnoti, G., Rosnay, P., Rozum, I., Vamborg, F., Villaume, S., Thépaut, J. N., Muñoz-Sabater, J., Nicolas, J., Peubey, C., Radu, R., Schepers, D., Simmons, A., Soci, C., Abdalla, S., Abellan, X., Balsamo, G., Bechtold, P., Biavati, G., Bidlot, J., Bonavita, M., De Chiara, G., Dahlgren, P., Dee, D., Diamantakis, M., Dragani, R., Flemming, J., Forbes, R., Fuentes, M., Geer, A., Haimberger, L., Healy, S., Hogan, R. J., Hólm, E., Janisková, M., Keeley, S., Laloyaux, P., Lopez, P., Lupu, C., Radnoti, G., de Rosnay, P., Rozum, I., Vamborg, F., Villaume, S., and Thépaut, J. N.: The ERA5 global reanalysis, *Quart. J. Roy. Meteorol. Soc.*, 146, 1999–2049, <https://doi.org/10.1002/qj.3803>, 2020.



- IEC: IEC 61400-1 Ed4: Wind turbines - Part 1: Design requirements, standard, International Electrotechnical Commission, Geneva, Switzerland, 2019.
- Imberger, M. and Larsén, X.: Sensitivity and quality assessment of the global 50-year return winds using reanalysis products and measurements., WindEurope Annual Event 2022, 2022.
- 380 IPCC: Climate Change 2021: The Physical Science Basis. Contribution of Working Group I to the Sixth Assessment Report of the Intergovernmental Panel on Climate Change, vol. In Press., Cambridge University Press, Cambridge, United Kingdom, and New York, USA, <https://www.ipcc.ch/report/ar6/wg1/>, 2021.
- Kawai, H., Yukimoto, S., Koshiro, T., Oshima, N., Tanaka, T., Yoshimura, H., and Nagasawa, R.: Significant improvement of cloud representation in the global climate model MRI-ESM2, Geoscientific Model Development, 12, 2875–2897, [https://doi.org/10.5194/gmd-12-2875-](https://doi.org/10.5194/gmd-12-2875-2019)  
385 2019, 2019.
- Larsén, X. and Mann, J.: Extreme Winds from the NCEP/NCAR Reanalysis Data, Wind Energy, 12, 556–573, <https://doi.org/10.1002/we.318>, 2009.
- Larsén, X. G. and Kruger, A.: Application of the spectral correction method to reanalysis data in South Africa, J. Wind Eng. Ind. Aerodyn.,  
390 133, 110–122, 2014.
- Larsén, X. G., Du, J., Bolanos, R., Imberger, M., Kelly, M., Badger, M., and Larsen, S.: Estimation of offshore extreme wind from wind-wave coupled modeling, Wind Energy, 22, 1043–1057, <https://doi.org/https://doi.org/10.1002/we.2339>, 2019.
- Larsén, X. and Mann, J.: The effects of disjunct sampling and averaging time on mean maximum wind, J. Wind Eng. Ind. Aerodyn, 94, 581–602, 2006.
- 395 Larsén, X., Kruger, A., Floors, R., Cavar, D., and Hahmann, A.: Extreme gust atlas over South Africa, EGU General Assembly 2021, online, 19–30 Apr 2021, EGU21-5829, <https://doi.org/https://doi.org/10.5194/egusphere-egu21-5829>, 2021.
- Larsén, X. G., Ott, S., Badger, J., Hahmann, A. H., and Mann, J.: Recipes for correcting the impact of effective mesoscale resolution on the estimation of extreme winds, J. Appl. Meteorol. Climat., 51, 521–533, <https://doi.org/10.1175/JAMC-D-11-090.1>, 2012.
- Larsén, X. G., Vincent, C. L., and Larsen, S.: Spectral structure of the mesoscale winds over the water, Q. J. R. Meteorol. Soc., 139, 685–700,  
400 <https://doi.org/DOI:10.1002/qj.2003>, 2013.
- Larsén, X. G., Davis, N., Hannesdottir, A., Kelly, M., Svenningsen, L., Slot, R., Imberger, M., Olsen, B., and Floors, R.: The Global Atlas for Siting Parameters (GASP) project: extreme wind, turbulence and turbine classes, Wind Energy, published online, <https://doi.org/10.1002/we.2771>, 2022.
- Mauritsen, T., Bader, J., Becker, T., Behrens, J., Bittner, M., Brokopf, R., Brovkin, V., Claussen, M., Crueger, T., Esch, M., Fast, I., Fiedler, S., Fläschner, D., Gayler, V., Giorgetta, M., Goll, D. S., Haak, H., Hagemann, S., Hedemann, C., Hohenegger, C., Ilyina, T., Jahns, T., Jimenéz-de-la Cuesta, D., Jungclaus, J., Kleinen, T., Kloster, S., Kracher, D., Kinne, S., Kleberg, D., Lasslop, G., Kornbluh, L., Marotzke, J., Matei, D., Meraner, K., Mikolajewicz, U., Modali, K., Möbis, B., Müller, W. A., Nabel, J. E. M. S., Nam, C. C. W., Notz, D., Nyawira, S.-S., Paulsen, H., Peters, K., Pincus, R., Pohlmann, H., Pongratz, J., Popp, M., Raddatz, T. J., Rast, S., Redler, R., Reick, C. H., Rohrschneider, T., Schemann, V., Schmidt, H., Schnur, R., Schulzweida, U., Six, K. D., Stein, L., Stemmler, I., Stevens, B., von  
410 Storch, J.-S., Tian, F., Voigt, A., Vrese, P., Wieners, K.-H., Wilkenskjeld, S., Winkler, A., and Roeckner, E.: Developments in the MPI-M Earth System Model version 1.2 (MPI-ESM1.2) and Its Response to Increasing CO<sub>2</sub>, Journal of Advances in Modeling Earth Systems, 11, 998–1038, <https://doi.org/https://doi.org/10.1029/2018MS001400>, 2019.
- MunichRe: Natural catastrophes 2011 analyses assessments positions, Munich Reinsurance Company Publications, 2011.



- Müller, W. A., Jungclaus, J. H., Mauritsen, T., Baehr, J., Bittner, M., Budich, R., Bunzel, F., Esch, M., Ghosh, R., Haak, H., Ilyina, T.,  
415 Kleine, T., Kornblueh, L., Li, H., Modali, K., Notz, D., Pohlmann, H., Roeckner, E., Stemmler, I., Tian, F., and Marotzke, J.: A Higher-  
resolution Version of the Max Planck Institute Earth System Model (MPI-ESM1.2-HR), *Journal of Advances in Modeling Earth Systems*,  
10, 1383–1413, <https://doi.org/https://doi.org/10.1029/2017MS001217>, 2018.
- NIKULIN, G., KJELLSTRÖM, E., HANSSON, U., STRANDBERG, G., and ULLERSTIG, A.: Evaluation and future projections of  
temperature, precipitation and wind extremes over Europe in an ensemble of regional climate simulations, *Tellus A*, 63, 41–55,  
420 <https://doi.org/https://doi.org/10.1111/j.1600-0870.2010.00466.x>, 2011.
- Outten, S. and Esau, I.: Extreme winds over Europe in the ENSEMBLES regional climate models, *Atmos. Chem. Phys.*, 13, 5163–5172,  
<https://doi.org/10.5194/acp-13-5163-2013>, 2013.
- Outten, S. and Sobolowski, S.: Extreme wind projections over Europe from the Euro-CORDEX regional climate models, *Weather and  
Climate Extremes*, 33, 100 363, <https://doi.org/https://doi.org/10.1016/j.wace.2021.100363>, 2021.
- 425 Pryor, S. and Bartelmie, R. J.: A global assessment of extreme wind speeds for wind energy applications, *Nature Energy*,  
<https://doi.org/https://doi.org/10.1038/s41560-020-00773-7>, 2021.
- Pryor, S. C., Barthelmie, R. J., Clausen, N. E., Drews, M., MacKeller, N., and Kjellstrom, E.: Analysis of possible changes in intense and  
extreme wind speeds over northern Europe under climate change scenarios., *Climate Dyn.*, 38, p. 189–208, 2012.
- Rockel, B. and Woth, K.: Extremes of near-surface wind speed over Europe and their future changes as estimated from an ensemble of RCM  
430 simulations, *Climatic Change* 81, pp. 267–280, 2007.
- Saha, S., Moorthi, S., Pan, H.-L., Wu, X., Wang, J., Nadiga, S., Tripp, P., Kistler, R., Woollen, J., Behringer, D., Liu, H., Stokes, D., Grumbine,  
R., Gayno, G., Wang, J., Hou, Y.-T., ya Chuang, H., Juang, H.-M. H., Sela, J., Iredell, M., Treadon, R., Kleist, D., Delst, P. V., Keyser,  
D., Derber, J., Ek, M., Meng, J., Wei, H., Yang, R., Lord, S., van den Dool, H., Kumar, A., Wang, W., Long, C., Chelliah, M., Xue,  
Y., Huang, B., Schemm, J.-K., Ebisuzaki, W., Lin, R., Xie, P., Chen, M., Zhou, S., Higgins, W., Zou, C.-Z., Liu, Q., Chen, Y., Han, Y.,  
435 Cucurull, L., Reynolds, R. W., Rutledge, G., and Goldberg, M.: The NCEP Climate Forecast System Reanalysis, *Bulletin of the American  
Meteorological Society*, 91, 1015 – 1058, <https://doi.org/10.1175/2010BAMS3001.1>, 2010.
- Schwierz, C., Kollner-Heck, P., Mutter, E., Bresch, D., Vidale, P., Wild, M., and Schär, C.: Modelling European winter wind storm losses  
in current and future climate, *Climatic Change* 101, pp. 485–514, 2010.
- Seland, Ø., Bentsen, M., Olivíé, D., Toniazzo, T., Gjermundsen, A., Graff, L. S., Debernard, J. B., Gupta, A. K., He, Y.-C., Kirkevåg,  
440 A., Schwinger, J., Tjiputra, J., Aas, K. S., Bethke, I., Fan, Y., Griesfeller, J., Grini, A., Guo, C., Ilicak, M., Karset, I. H. H., Landgren,  
O., Liakka, J., Moseid, K. O., Nummelin, A., Spensberger, C., Tang, H., Zhang, Z., Heinze, C., Iversen, T., and Schulz, M.: Overview  
of the Norwegian Earth System Model (NorESM2) and key climate response of CMIP6 DECK, historical, and scenario simulations,  
*Geoscientific Model Development*, 13, 6165–6200, <https://doi.org/10.5194/gmd-13-6165-2020>, 2020.
- Sellar, A. A., Walton, J., Jones, C. G., Wood, R., Abraham, N. L., Andrejczuk, M., Andrews, M. B., Andrews, T., Archibald, A. T., de Mora,  
445 L., Dyson, H., Elkington, M., Ellis, R., Florek, P., Good, P., Gohar, L., Haddad, S., Hardiman, S. C., Hogan, E., Iwi, A., Jones, C. D.,  
Johnson, B., Kelley, D. I., Kettleborough, J., Knight, J. R., Köhler, M. O., Kuhlbrodt, T., Liddicoat, S., Linova-Pavlova, I., Mizieliński,  
M. S., Morgenstern, O., Mulcahy, J., Neining, E., O’Connor, F. M., Petrie, R., Ridley, J., Rioual, J.-C., Roberts, M., Robertson,  
E., Rumbold, S., Seddon, J., Shepherd, H., Shim, S., Stephens, A., Teixeira, J. C., Tang, Y., Williams, J., Wiltshire, A., and Griffiths,  
P. T.: Implementation of U.K. Earth System Models for CMIP6, *Journal of Advances in Modeling Earth Systems*, 12, e2019MS001 946,  
450 <https://doi.org/https://doi.org/10.1029/2019MS001946>, e2019MS001946 10.1029/2019MS001946, 2020.



- Smith, D., Scaife, A., and Eade, R. e. a.: North Atlantic climate far more predictable than models imply, *Nature*, pp. 796–800, <https://doi.org/https://doi.org/10.1038/s41586-020-2525-0>, 2020.
- Swart, N. C., Cole, J. N. S., Kharin, V. V., Lazare, M., Scinocca, J. F., Gillett, N. P., Anstey, J., Arora, V., Christian, J. R., Hanna, S., Jiao, Y., Lee, W. G., Majaess, F., Saenko, O. A., Seiler, C., Seinen, C., Shao, A., Sigmond, M., Solheim, L., von Salzen, K., Yang, D., and Winter, B.: The Canadian Earth System Model version 5 (CanESM5.0.3), *Geoscientific Model Development*, 12, 4823–4873, <https://doi.org/10.5194/gmd-12-4823-2019>, 2019.
- 455 S  f  rian, R., Nabat, P., Michou, M., Saint-Martin, D., Voldoire, A., Colin, J., Decharme, B., Delire, C., Berthet, S., Chevallier, M., S  n  si, S., Franchisteguy, L., Vial, J., Mallet, M., Joetzer, E., Geoffroy, O., Gu  r  my, J.-F., Moine, M.-P., Msadek, R., Ribes, A., Rocher, M., Roehrig, R., Salas-y M  lia, D., Sanchez, E., Terray, L., Valcke, S., Waldman, R., Aumont, O., Bopp, L., Deshayes, J.,   th  , C., and
- 460 Madec, G.: Evaluation of CNRM Earth System Model, CNRM-ESM2-1: Role of Earth System Processes in Present-Day and Future Climate, *Journal of Advances in Modeling Earth Systems*, 11, 4182–4227, <https://doi.org/https://doi.org/10.1029/2019MS001791>, 2019.
- Tatebe, H., Ogura, T., Nitta, T., Komuro, Y., Ogochi, K., Takemura, T., Sudo, K., Sekiguchi, M., Abe, M., Saito, F., Chikira, M., Watanabe, S., Mori, M., Hirota, N., Kawatani, Y., Mochizuki, T., Yoshimura, K., Takata, K., O’ishi, R., Yamazaki, D., Suzuki, T., Kurogi, M., Kataoka, T., Watanabe, M., and Kimoto, M.: Description and basic evaluation of simulated mean state, internal variability, and climate sensitivity
- 465 in MIROC6, *Geoscientific Model Development*, 12, 2727–2765, <https://doi.org/10.5194/gmd-12-2727-2019>, 2019.
- Taylor, K. E., Stouffer, R. J., and Meehl, G. A.: An Overview of CMIP5 and the Experiment Design, *Bull. Amer. Meteorol. Soc.*, 93, 485–498, <https://doi.org/10.1175/BAMS-D-11-00094.1>, 2012.
- Tilo, Z., A., C. M., M., L. R., Andrew, L., W., B. R., Martin, D., Lauren, S., Ying-Ping, W., and Jhan, S.: The Australian Earth System Model: ACCESS-ESM1.5, *J. of Southern Hemisphere Earth Systems Science*, 70, 193–214, <https://doi.org/10.1071/ES19035>, 2020.
- 470 Voldoire, A., Saint-Martin, D., S  n  si, S., Decharme, B., Alias, A., Chevallier, M., Colin, J., Gu  r  my, J.-F., Michou, M., Moine, M.-P., Nabat, P., Roehrig, R., Salas y M  lia, D., S  f  rian, R., Valcke, S., Beau, I., Belamari, S., Berthet, S., Cassou, C., Cattiaux, J., Deshayes, J., Douville, H., Eth  , C., Franchist  guy, L., Geoffroy, O., L  vy, C., Madec, G., Meurdesoif, Y., Msadek, R., Ribes, A., Sanchez-Gomez, E., Terray, L., and Waldman, R.: Evaluation of CMIP6 DECK Experiments With CNRM-CM6-1, *Journal of Advances in Modeling Earth Systems*, 11, 2177–2213, <https://doi.org/https://doi.org/10.1029/2019MS001683>, 2019.
- 475 Yang, Y., Wang, B., and Cao, J. e. a.: Improved historical simulation by enhancing moist physical parameterizations in the climate system model NESM3.0., *Clim Dyn*, 54, 3819–3840, <https://doi.org/10.1007/s00382-020-05209-2>, 2020.